IEEE Access
Multidisciplinary | Rapid Review | Open Access Journal

Received September 24, 2019, accepted October 10, 2019, date of publication October 15, 2019, date of current version October 28, 2019.

Digital Object Identifier 10.1109/ACCESS.2019.2947467

In-Service Blind Transceiver IQ Imbalance and Skew Monitoring in Long-Haul Non-Dispersion Managed Coherent Optical Systems

CHENG JU, NA LIU, AND CHANGHONG LI
College of Electronic Information, Qingdao University, Qingdao 266071, China
Corresponding author: Cheng Ju (jucheng719@qdu.edu.cn)

This work was supported in part by the National Natural Science Foundation of China under Grant 61701271, and in part by the Open Fund of IPOC (BUPT).

ABSTRACT Transceiver imbalance can rapidly degrade system performance, especially when high symbol rate, high modulation order and low roll-off pulse shape are used. Here, a widely linear transmission model is derived to analyze the interaction of transceiver IQ gain imbalance, IQ phase imbalance, skew and fiber link for long-haul transmission. In-service blind transceiver imbalance measurement method is designed to calibrate and monitor the transceiver status. Two 4×2 complex-valued equalizers operated at twice symbol rates are designed before and after carrier phase recovery (CPR) to compensate receiver and transmitter imbalances, where the transceiver imbalance could be derived from the taps of two converged equalizers. The impact of transceiver imbalance and fiber nonlinearity on the measurement accuracy are numerically evaluated based on a 42 GBaud 16-QAM system through 1500-km standard single fiber (SSMF) transmission.

INDEX TERMS Transceiver IQ imbalance, skew, in-service blind monitoring, coherent optical systems.

I. INTRODUCTION

Coherent optical communication has been rapidly developed owing to its ability to improve receiver sensitivity, spectral efficiency, as well as to mitigate the transmission impairments by using digital signal processing (DSP) [1]. Increasing the symbol rate and modulation order as well as the use of roll-off factor close to zero is a natural and practical way to increase the system capacity. However, the system performance would be vulnerable to the transceiver imbalance, including gain imbalance, phase imbalance and skew. Receiver imbalance compensation and calibration methods are well discussed in the literatures, including Gram-Schmidt orthogonalization procedure for gain and phase imbalance compensation [2], 4×2 complex-valued equalizer for gain, phase imbalance and skew compensation and calibration [3], [4], 4×4 real-valued equalizer for gain, phase imbalance and skew compensation [5], [6], modified interpolator in timing recovery for skew compensation and calibration [7], off-line beat frequency skew calibration method agreed by Optical Internetworking Forum (OIF) [8] and modified beat frequency method with iteration for skew calibration [9]. Transmitter imbalance is more critical for transmission and some recent works have attempted for compensation and calibration, such as indirect learning architecture-based skew calibration method for back-to-back case [10], 2×2 real-valued equalizer for imbalance compensation and calibration [11], adaptive source separation method for gain and phase imbalance compensation [12], off-line skew self-calibration with integrated low-bandwidth photodetector in commercial IQ modulator [13], reconfigurable interference method for skew calibration [14], clock tone extraction based on genetic algorithm for skew calibration [15], and clustering algorithm based gain and phase imbalance estimation [16]. Nevertheless, to the author's best knowledge, no explicit model has been given to analyze the interaction of transceiver imbalance and fiber linear interference in long-haul transmission scenario.

Due to the introduction of CFP2 for analogue coherent optics (CFP2-ACO) hot pluggable modules [8], the ACO module and DSP chip could be supplied by different vendor, which provides more options for operators. The distinct advantage is that the defective ACO module could be

The associate editor coordinating the review of this manuscript and approving it for publication was Qilian Liang.

easily exchanged. ACO modules from different vendors have different device characteristics, and the device parameters are varied due to module temperature, wavelength, amplifier gain and aging. Hence, to achieve the optimal performance, transceiver calibration is necessary especially for high baud rate and high order modulation systems. Moreover, it is expected that optical transceiver has a monitor function, which can estimate and locate the imperfect device when system performance decline. Compared with off-line or factory calibration, in-service method is more attractive for real time monitoring and calibration. In-service blind estimation of transceiver imbalance is preferred for long-haul non-dispersion managed system.

As main contribution of this work, theory model is derived based on widely linear transformation to explore the interaction between fiber link and transceiver imbalance. Widely linear equalizer based on stochastic gradient descent for taps updating can only compensate quasi-static interference, such as polarization-mode dispersion (PMD), chromatic dispersion (CD) and receiver imbalance, but can not track and compensate fast time-varying interference, such as frequency offset and laser phase noise. Based on the analysis model, two 4×2 complex-valued equalizers operating at two samples per symbol are utilized before and after CPR to mitigate receiver and transmitter imbalance, and the transceiver gain imbalance, phase imbalance and skew can be extracted from the converged tap coefficients. Detailed analysis would be given to explain why these equalization architectures are more suitable for in-service imbalance calibration rather than imbalance compensation. Finally, the performance and estimation accuracy are investigated in a 42 GBaud polarization division multiplexing (PDM) 16-QAM simulation system after 1500-km SSMF transmission. The effect of transmitter imbalance on receiver imbalance estimation, the effect of receiver imbalance on transmitter imbalance estimation, and the effect of fiber nonlinearity on transceiver imbalance estimation are evaluated in the following.

II. THEORETICAL MODELING AND IMBALANCE MONITORING

The channel modeling is derived in the following three cases: 1) without transceiver imbalance, 2) with only receiver imbalance, 3) with transceiver imbalance. In the following description, equalizer refers to the time domain processing unless mentioned otherwise.

First, in absence of transceiver imbalance, the received signals of I and Q branches in frequency domain can be represented as $\mathrm{XI}(\omega)$ and $\mathrm{XQ}(\omega)$, $\mathrm{YI}(\omega)$ and $\mathrm{YQ}(\omega)$ for the X and Y polarizations, respectively. Then, the received optical filed signals are reconstructed as $\mathrm{X}(\omega) = \mathrm{XI}(\omega) + 1\mathrm{j} * \mathrm{XQ}(\omega)$ and $\mathrm{Y}(\omega) = \mathrm{YI}(\omega) + 1\mathrm{j} * \mathrm{YQ}(\omega)$. The transmission without transceiver imbalance can be completely described by strictly linear complex-valued model. The processes of CD compensation and conventional 2×2 equalizer can be expressed as equation (1), as shown at the bottom of this page, where $\hat{\theta}_{CD}(\omega)$ is the estimated dispersion factor at angle frequency of ω, $H_{X\_X}(\omega)$, $H_{Y\_X}(\omega)$, $H_{X\_Y}(\omega)$ and $H_{Y\_Y}(\omega)$ are the discrete Fourier transform (DFT) of 2×2 equalizer taps, $h_{X\_X}(t)$, $h_{Y\_X}(t)$, $h_{X\_Y}(t)$ and $h_{Y\_Y}(t)$. This structure with two CD compensators and one 2×2 equalizer enforces joint filtering the I and Q components and it belongs to the category of strictly linear transformation [4]. Four CD compensators and one complex-valued 4×2 equalizers are introduced to separate filtering I and Q components [6]. Hence, it is also possible to rewrite (1) as (2), as shown at the bottom of this page, where a four-by-four matrix $H_{CD}(\omega)$ used for CD compensation is

$$H_{CD}(\omega) = \begin{bmatrix} e^{j\hat{\theta}_{CD}(\omega)} & 0 & 0 & 0 \\ 0 & e^{j\hat{\theta}_{CD}(\omega)} & 0 & 0 \\ 0 & 0 & e^{j\hat{\theta}_{CD}(\omega)} & 0 \\ 0 & 0 & 0 & e^{j\hat{\theta}_{CD}(\omega)} \end{bmatrix}. \tag{3}$$

Second, we consider the case that only receiver imbalance is included. Let I branch as a reference, α_{RX} and α_{RY}, δ_{RX} and δ_{RY}, τ_{RX} and τ_{RY} are the gain imbalance, phase imbalance and skew of Q branch for X and Y Pol. The received signal can be written as $\begin{bmatrix} 1 & 0 \\ 0 & e^{j\omega\tau_{RX}} \end{bmatrix}\begin{bmatrix} 1 & 0 \\ -sin\delta_{RX} & cos\delta_{RX} \end{bmatrix}\begin{bmatrix} 1 & 0 \\ 0 & \alpha_{RX} \end{bmatrix}\begin{bmatrix} \mathrm{XI}(\omega) \\ \mathrm{XQ}(\omega) \end{bmatrix}$ and $\begin{bmatrix} 1 & 0 \\ 0 & e^{j\omega\tau_{RY}} \end{bmatrix}\begin{bmatrix} 1 & 0 \\ -sin\delta_{RY} & cos\delta_{RY} \end{bmatrix}\begin{bmatrix} 1 & 0 \\ 0 & \alpha_{RY} \end{bmatrix}\begin{bmatrix} \mathrm{YI}(\omega) \\ \mathrm{YQ}(\omega) \end{bmatrix}$. Then, the processes of CD compensator and 4×2 equalizer can be written as

$$\begin{bmatrix} \mathrm{X}_{out}(\omega) \\ \mathrm{Y}_{out}(\omega) \end{bmatrix} = H_{EQ}^{4\times2}(\omega) H_{CD}(\omega) H_R(\omega) \begin{bmatrix} \mathrm{XI}(\omega) \\ \mathrm{XQ}(\omega) \\ \mathrm{YI}(\omega) \\ \mathrm{YQ}(\omega) \end{bmatrix}, \tag{4}$$

where $H_R(\omega)$ is a four-by-four matrix describing receiver imbalance shown in (5), as shown at the bottom of

$$\begin{bmatrix} \mathrm{X}_{out}(\omega) \\ \mathrm{Y}_{out}(\omega) \end{bmatrix} = \begin{bmatrix} H_{X\_X}(\omega) & H_{Y\_X}(\omega) \\ H_{X\_Y}(\omega) & H_{Y\_Y}(\omega) \end{bmatrix}\begin{bmatrix} e^{j\hat{\theta}_{CD}(\omega)} & 0 \\ 0 & e^{j\hat{\theta}_{CD(\omega)}} \end{bmatrix}\begin{bmatrix} \mathrm{X}(\omega) \\ \mathrm{Y}(\omega) \end{bmatrix}. \tag{1}$$

$$\begin{bmatrix} \mathrm{X}_{out}(\omega) \\ \mathrm{Y}_{out}(\omega) \end{bmatrix} = \begin{bmatrix} H_{X\_X}(\omega) & jH_{X\_X}(\omega) & H_{Y\_X}(\omega) & jH_{Y\_X}(\omega) \\ H_{X\_Y}(\omega) & jH_{X\_Y}(\omega) & H_{Y\_Y}(\omega) & jH_{Y\_Y}(\omega) \end{bmatrix} H_{CD}(\omega) \begin{bmatrix} \mathrm{XI}(\omega) \\ \mathrm{XQ}(\omega) \\ \mathrm{YI}(\omega) \\ \mathrm{YQ}(\omega) \end{bmatrix}. \tag{2}$$

this page, and $H_{EQ}^{4\times2}(\omega)$ is a two-by-four transfer matrix describing the operation of 4×2 equalizer.

$$H_{EQ}^{4\times2}(\omega) = \begin{bmatrix} H_{XI\_X}(\omega) & jH_{XQ\_X}(\omega) & H_{YI\_X}(\omega) & jH_{YQ\_X}(\omega) \\ H_{XI\_Y}(\omega) & jH_{XQ\_Y}(\omega) & H_{YI\_Y}(\omega) & jH_{YQ\_Y}(\omega) \end{bmatrix}. \quad (6)$$

$H_{XI\_X}(\omega)$, $H_{XQ\_X}(\omega)$, $H_{YI\_X}(\omega)$, $H_{YQ\_X}(\omega)$, $H_{XI\_Y}(\omega)$, $H_{XQ\_Y}(\omega)$, $H_{YI\_Y}(\omega)$ and $H_{YQ\_Y}(\omega)$ are the DFT of 4×2 equalizer taps $h_{XI\_X}(t)$, $h_{XQ\_X}(t)$, $h_{YI\_X}(t)$, $h_{YQ\_X}(t)$, $h_{XI\_Y}(t)$, $h_{XQ\_Y}(t)$, $h_{YI\_Y}(t)$ and $h_{YQ\_Y}(t)$. Thus, from Eq. (2) and (4), it is possible to obtain

$$H_{XI\_X}(\omega) = \left(1 + j\frac{sin\delta_{RX}}{\alpha_{RX}cos\delta_{RX}}\right) H_{X\_X}(\omega), \quad (7)$$

$$H_{XQ\_X}(\omega) = \left(\frac{1}{\alpha_{RX}cos\delta_{RX}e^{j\omega\tau_{RX}}}\right) H_{X\_X}(\omega), \quad (8)$$

$$H_{YI\_X}(\omega) = \left(1 + j\frac{sin\delta_{RY}}{\alpha_{RY}cos\delta_{RY}}\right) H_{Y\_X}(\omega), \quad (9)$$

$$H_{YQ\_X}(\omega) = \left(\frac{1}{\alpha_{RY}cos\delta_{RY}e^{j\omega\tau_{RY}}}\right) H_{Y\_X}(\omega), \quad (10)$$

$$H_{XI\_Y}(\omega) = \left(1 + j\frac{sin\delta_{RX}}{\alpha_{RX}cos\delta_{RX}}\right) H_{X\_Y}(\omega), \quad (11)$$

$$H_{XQ\_Y}(\omega) = \left(\frac{1}{\alpha_{RX}cos\delta_{RX}e^{j\omega\tau_{RX}}}\right) H_{X\_Y}(\omega), \quad (12)$$

$$H_{YI\_Y}(\omega) = \left(1 + j\frac{sin\delta_{RY}}{\alpha_{RY}cos\delta_{RY}}\right) H_{Y\_Y}(\omega), \quad (13)$$

and

$$H_{YQ\_Y}(\omega) = \left(\frac{1}{\alpha_{RY}cos\delta_{RY}e^{j\omega\tau_{RY}}}\right) H_{Y\_Y}(\omega). \quad (14)$$

Receiver imbalance information is contained in the frequency response difference with filters coming from the same polarization and going to the same polarization. Frequency response difference between $H_{XI\_X}(\omega)$ and $H_{XQ\_X}(\omega)$, $H_{XI\_Y}(\omega)$ and $H_{XQ\_Y}(\omega)$, $H_{YI\_X}(\omega)$ and $H_{YQ\_X}(\omega)$, $H_{YI\_Y}(\omega)$ and $H_{YQ\_Y}(\omega)$ are

$$\frac{H_{XI\_X}(\omega)}{H_{XQ\_X}(\omega)} = \left(1 + j\frac{sin\delta_{RX}}{\alpha_{RX}cos\delta_{RX}}\right)\alpha_{RX}cos\delta_{RX}e^{j\omega\tau_{RX}}, \quad (15)$$

$$\frac{H_{XI\_Y}(\omega)}{H_{XQ\_Y}(\omega)} = \left(1 + j\frac{sin\delta_{RX}}{\alpha_{RX}cos\delta_{RX}}\right)\alpha_{RX}cos\delta_{RX}e^{j\omega\tau_{RX}}, \quad (16)$$

$$\frac{H_{YI\_X}(\omega)}{H_{YQ\_X}(\omega)} = \left(1 + j\frac{sin\delta_{RY}}{\alpha_{RY}cos\delta_{RY}}\right)\alpha_{RY}cos\delta_{RY}e^{j\omega\tau_{RY}}, \quad (17)$$

and

$$\frac{H_{YI\_Y}(\omega)}{H_{YQ\_Y}(\omega)} = \left(1 + j\frac{sin\delta_{RY}}{\alpha_{RY}cos\delta_{RY}}\right)\alpha_{RY}cos\delta_{RY}e^{j\omega\tau_{RY}}. \quad (18)$$

Energy of converged taps varies in real time due to randomness of polarization rotation. The taps with high energy in Eq. (15) and (16), (17) and (18) are used to calculate imbalance for X and Y Pol., respectively. Receiver gain imbalance could be estimated from the following equations,

$$\alpha_{RX} \approx E\left[\left|\frac{H_{XI\_X}(\omega)}{H_{XQ\_X}(\omega)}\right|\right] = \mathrm{E}\left[\left|\frac{H_{XI\_Y}(\omega)}{H_{XQ\_Y}(\omega)}\right|\right] \quad (19)$$

and

$$\alpha_{RY} \approx E\left[\left|\frac{H_{YI\_X}(\omega)}{H_{YQ\_X}(\omega)}\right|\right] = \mathrm{E}\left[\left|\frac{H_{YI\_Y}(\omega)}{H_{YQ\_Y}(\omega)}\right|\right]. \quad (20)$$

where $E[.]$ represents the average operation. For Nyquist signal, the average operation is only performed for intra band frequency. The phases of frequency response differences are described by

$$\varphi_X(\omega) = arctan\frac{sin\delta_{RX}}{\alpha_{RX}cos\delta_{RX}} + \omega\tau_{RX} \quad (21)$$

and

$$\varphi_Y(\omega) = arctan\frac{sin\delta_{RY}}{\alpha_{RY}cos\delta_{RY}} + \omega\tau_{RY}. \quad (22)$$

$\varphi_X(\omega)$ and $\varphi_Y(\omega)$ are the linear variation of phase as a function of angle frequency, ω. The skew is proportional to the slope of this phase in intra band frequency. When $\omega = 0$, receiver phase imbalance can be calculated by

$$\delta_{RX} = arctan\{\alpha_{RX}tan[\varphi_X(0)]\} \quad (23)$$

and

$$\delta_{RY} = arctan\{\alpha_{RY}tan[\varphi_Y(0)]\}. \quad (24)$$

An effective way to calculate the skew and phase imbalance is doing a linear regression [3] of phase $\varphi_X(\omega)$ and $\varphi_Y(\omega)$ to find the slope and phase value with $\omega = 0$.

Third, we consider the case that transceiver imbalance is involved. Transmitter transfer matrix could be written as (25), as shown at the bottom of the next page, where α_{TX} and α_{TY}, δ_{TX} and δ_{TY}, τ_{TX} and τ_{TY} are the gain imbalance, phase imbalance and skew of Q branch relative to I branch for X and Y Pol., respectively. Fiber channel transfer matrix described by strictly linear complex-valued model can be written in time domain as $\begin{bmatrix} q_{X\_X}(t) & q_{Y\_X}(t) \\ q_{X\_Y}(t) & q_{Y\_Y}(t) \end{bmatrix}$, which involves the overall effects of polarization crosstalk, differential group delay (DGD) and polarization dependent loss (PDL), and also can be rewritten in real-valued matrix form as (26), as shown at the bottom of the next page. $Q(t)$ can be written in the frequency domain as (27), as shown at the bottom of the next page, where $\mathcal{F}$ represents the DFT operation.

$$H_R(\omega) = \begin{bmatrix} 1 & 0 & 0 & 0 \\ -sin\delta_{RX}e^{j\omega\tau_{RX}} & \alpha_{RX}cos\delta_{RX}e^{j\omega\tau_{RX}} & 0 & 0 \\ 0 & 0 & 1 & 0 \\ 0 & 0 & -sin\delta_{RY}e^{j\omega\tau_{RY}} & \alpha_{RY}cos\delta_{RY}e^{j\omega\tau_{RY}} \end{bmatrix} \quad (5)$$

The transfer matrixes of CD and phase rotation caused by frequency offset and phase noise can be written in four-by-four form as (28) and (29), as shown at the bottom of this page, where $\theta_{CD}(\omega)$ is the phase shift caused by CD at angle frequency of ω, $\Delta\omega$ is transceiver frequency offset and $\theta(t)$ is phase noise caused by laser linewidth. Therefore, the overall transfer function of the fiber link, CD compensator and 4×2 equalizer can be expressed as (30), as shown at the bottom of this page, where $\mathrm{XI}_T(\omega)$, $\mathrm{XQ}_T(\omega)$, $\mathrm{YI}_T(\omega)$ and $\mathrm{YQ}_T(\omega)$ are the DFT of transmitted ideal signal at XI, XQ, YI and YQ branches, respectively.

Considering the case that $\theta_{CD}(\omega) \approx \hat{\theta}_{CD}(\omega)$, four static CD compensators $H_{CD}(\omega)$ can roughly accomplish CD compensation, and the residual CD can be handled by the following 4×2 equalizer. For long-haul transmission, CD, PDL and DGD are pretty stable, while the state-of-polarization (SOP) experiences fast variations of several tens of krad/s. Generally, 4×2 equalizer based on radius

$$H_T(\omega) = \begin{bmatrix} 1 & 0 & 0 & 0 \\ -sin\delta_{TX}e^{j\omega\tau_{TX}} & \alpha_{TX}cos\delta_{TX}e^{j\omega\tau_{TX}} & 0 & 0 \\ 0 & 0 & 1 & 0 \\ 0 & 0 & -sin\delta_{TY}e^{j\omega\tau_{TY}} & \alpha_{TY}cos\delta_{TY}e^{j\omega\tau_{TY}} \end{bmatrix}. \tag{25}$$

$$Q(t) = \begin{bmatrix} Re[q_{X\_X}(t)] & -Im[q_{X\_X}(t)] & Re[q_{Y\_X}(t)] & -Im[q_{Y\_X}(t)] \\ Im[q_{X\_X}(t)] & Re[q_{X\_X}(t)] & Im[q_{Y\_X}(t)] & Re[q_{Y\_X}(t)] \\ Re[q_{X\_Y}(t)] & -Im[q_{X\_Y}(t)] & Re[q_{Y\_Y}(t)] & -Im[q_{Y\_Y}(t)] \\ Im[q_{X\_Y}(t)] & Re[q_{X\_Y}(t)] & Im[q_{Y\_Y}(t)] & Re[q_{Y\_Y}(t)] \end{bmatrix}. \tag{26}$$

$$\begin{aligned} Q(\omega) &= \begin{bmatrix} Q^R_{X\_X}(\omega) & -Q^I_{X\_X}(\omega) & Q^R_{Y\_X}(\omega) & -Q^I_{Y\_X}(\omega) \\ Q^I_{X\_X}(\omega) & Q^R_{X\_X}(\omega) & Q^I_{Y\_X}(\omega) & Q^R_{Y\_X}(\omega) \\ Q^R_{X\_Y}(\omega) & -Q^I_{X\_Y}(\omega) & Q^R_{Y\_Y}(\omega) & -Q^I_{Y\_Y}(\omega) \\ Q^I_{X\_Y}(\omega) & Q^R_{X\_Y}(\omega) & Q^I_{Y\_Y}(\omega) & Q^R_{Y\_Y}(\omega) \end{bmatrix} \\ &= \begin{bmatrix} \mathcal{F}\{Re[q_{X\_X}(t)]\} & -\mathcal{F}\{Im[q_{X\_X}(t)]\} & \mathcal{F}\{Re[q_{Y\_X}(t)]\} & -\mathcal{F}\{Im[q_{Y\_X}(t)]\} \\ \mathcal{F}\{Im[q_{X\_X}(t)]\} & \mathcal{F}\{Re[q_{X\_X}(t)]\} & \mathcal{F}\{Im[q_{Y\_X}(t)]\} & \mathcal{F}\{Re[q_{Y\_X}(t)]\} \\ \mathcal{F}\{Re[q_{X\_Y}(t)]\} & -\mathcal{F}\{Im[q_{X\_Y}(t)]\} & \mathcal{F}\{Re[q_{Y\_Y}(t)]\} & -\mathcal{F}\{Im[q_{Y\_Y}(t)]\} \\ \mathcal{F}\{Im[q_{X\_Y}(t)]\} & \mathcal{F}\{Re[q_{X\_Y}(t)]\} & \mathcal{F}\{Im[q_{Y\_Y}(t)]\} & \mathcal{F}\{Re[q_{Y\_Y}(t)]\} \end{bmatrix}, \end{aligned} \tag{27}$$

$$Q_{CD}(\omega) = \begin{bmatrix} e^{-j\theta_{CD}(\omega)} & 0 & 0 & 0 \\ 0 & e^{-j\theta_{CD}(\omega)} & 0 & 0 \\ 0 & 0 & e^{-j\theta_{CD}(\omega)} & 0 \\ 0 & 0 & 0 & e^{-j\theta_{CD}(\omega)} \end{bmatrix}, \tag{28}$$

$$P(\Delta\omega, t) = \begin{bmatrix} cos[\Delta\omega t + \theta(t)] & -sin[\Delta\omega t + \theta(t)] & 0 & 0 \\ sin[\Delta\omega t + \theta(t)] & cos[\Delta\omega t + \theta(t)] & 0 & 0 \\ 0 & 0 & cos[\Delta\omega t + \theta(t)] & -sin[\Delta\omega t + \theta(t)] \\ 0 & 0 & sin[\Delta\omega t + \theta(t)] & cos[\Delta\omega t + \theta(t)] \end{bmatrix}, \tag{29}$$

$$\begin{bmatrix} \mathrm{X}_{out}(\omega) \\ \mathrm{Y}_{out}(\omega) \end{bmatrix} = H^{4\times2}_{EQ}(\omega) H_{CD}(\omega) H_R(\omega) Q_{CD}(\omega) Q(\omega) P(\Delta\omega, t) H_T(\omega) \begin{bmatrix} \mathrm{XI}_T(\omega) \\ \mathrm{XQ}_T(\omega) \\ \mathrm{YI}_T(\omega) \\ \mathrm{YQ}_T(\omega) \end{bmatrix}, \tag{30}$$

$$\begin{aligned} H^{4\times4}_{EQ}(\omega) &= [H_{CD}(\omega) H_R(\omega) Q_{CD}(\omega) Q(\omega)]^{-1} \\ &= \begin{bmatrix} H^R_{XI\_X}(\omega) & -H^I_{XQ\_X}(\omega) & H^R_{YI\_X}(\omega) & -H^I_{YQ\_X}(\omega) \\ H^I_{XI\_X}(\omega) & H^R_{XQ\_X}(\omega) & H^I_{YI\_X}(\omega) & H^R_{YQ\_X}(\omega) \\ H^R_{XI\_Y}(\omega) & -H^I_{XQ\_Y}(\omega) & H^R_{YI\_Y}(\omega) & -H^I_{YQ\_Y}(\omega) \\ H^I_{XI\_Y}(\omega) & H^R_{XQ\_Y}(\omega) & H^I_{YI\_Y}(\omega) & H^R_{YQ\_Y}(\omega) \end{bmatrix} \\ &= \begin{bmatrix} \mathcal{F}\{Re[h_{XI\_X}(t)]\} & -\mathcal{F}\{Im[h_{XQ\_X}(t)]\} & \mathcal{F}\{Re[h_{YI\_X}(t)]\} & -\mathcal{F}\{Im[h_{YQ\_X}(t)]\} \\ \mathcal{F}\{Im[h_{XI\_X}(t)]\} & \mathcal{F}\{Re[h_{XQ\_X}(t)]\} & \mathcal{F}\{Im[h_{YI\_X}(t)]\} & \mathcal{F}\{Re[h_{YQ\_X}(t)]\} \\ \mathcal{F}\{Re[h_{XI\_Y}(t)]\} & -\mathcal{F}\{Im[h_{XQ\_Y}(t)]\} & \mathcal{F}\{Re[h_{YI\_Y}(t)]\} & -\mathcal{F}\{Im[h_{YQ\_Y}(t)]\} \\ \mathcal{F}\{Im[h_{XI\_Y}(t)]\} & \mathcal{F}\{Re[h_{XQ\_Y}(t)]\} & \mathcal{F}\{Im[h_{YI\_Y}(t)]\} & \mathcal{F}\{Re[h_{YQ\_Y}(t)]\} \end{bmatrix} \end{aligned} \tag{31}$$

directed equalizer (RDE) criteria can provide a precise and fast SOP tracking. Therefore, residual CD, PDL, DGD and receiver imbalance can be completely compensated by using 4×2 equalizer in theory. Inverse matrix of transfer function $H_{CD}(\omega) H_R(\omega) Q_{CD}(\omega) Q(\omega)$ can be expressed as (31), as shown at the bottom of the previous page, where $H_{EQ}^{4\times4}(\omega)$ is a four-by-four transfer matrix described the procedure of 4×4 equalizer. Without four CD compensators $H_{CD}(\omega)$, 4×4 equalizer has four real value inputs in time domain, which is the conventional 4×4 real-valued equalizer [5]. With $H_{CD}(\omega)$, the inputs of 4×4 equalizer are four complex values. Moreover, the tap coefficients of 4×4 equalizer are real value both for the case with and without $H_{CD}(\omega)$. 4×4 equalizer with real-valued tap coefficients can be equivalently represented as a 4×2 complex-valued equalizer with transfer matrix of $H_{EQ}^{4\times2}(\omega)$. $h_{XI\_X}(t)$, $h_{XQ\_X}(t)$, $h_{YI\_X}(t)$, $h_{YQ\_X}(t)$, $h_{XI\_Y}(t)$, $h_{XQ\_Y}(t)$, $h_{YI\_Y}(t)$ and $h_{YQ\_Y}(t)$ are the tap coefficients of 4×2 equalizer in time domain. Notably, the converged transfer matrix $H_{EQ}^{4\times4}(\omega)$ based on RDE or least mean square (LMS) criteria is also considered to satisfy the relation of Eq. (31). $P(\Delta\omega, t)$ in Eq. (30) experiences fast variations of Mrad/s or Grad/s, e.g. more than 628 Mrad/s for frequency offset of 100 MHz. However, tracking speed of 4×2 equalizer, which is limited by slow convergence of stochastic gradient descent criteria, DSP parallel processing and hardware logic delay, is far less than the variations of $P(\Delta\omega, t)$. It should be noted that the joint effect of $P(\Delta\omega, t) H_T(\omega)$ induces the rotation of constellation and the increasing of modulus ring thickness. From the above analysis, it is clear that the equalizer sequence for long-haul transmission is 1) four CD compensators, 2) RDE-based 4×2 equalizer to compensate the joint effect of $H_{CD}(\omega) H_R(\omega) Q_{CD}(\omega) Q(\omega)$, 3) CPR for $P(\Delta\omega, t)$, 4) decision-directed (DD) LMS-based 4×2 equalizer to deal with the impact of transmitter imbalance. Therefore, transmitter imbalance can also be estimated from the converged tap coefficients of DD-LMS-based 4×2 equalizer. It is necessary to notice that, to acquire optimal performance of transmitter imbalance compensation and estimation (especially for frequency dependent effect, such as skew), operating at twice symbol rates are needed for the two 4×2 equalizers and CPR module.

Although the above designed method may be used for transceiver imbalance compensation, its use in practical systems will be hindered by the additional computation complexity. Complexity is mainly manifested in the following aspects: 1) the complexity required for 4×2 equalizer will scale proportionally to twice the complexity of traditional 2×2 equalizer, 2) two 4×2 equalizers are needed before and after CPR, 3) processing of twice symbol rates is needed for the two 4×2 equalizers and CPR, which further doubles the complexity. Besides, transmitter imbalance reduces the accuracy of symbol decision in RDE-based taps updating, and impacts the performance of the first 4×2 equalizer. The residual receiver imbalance and channel linear interference further affects the performance of the second 4×2 equalizer, which would be analyzed in the following numerical simulation. From the above analysis, the author suggests that the traditional 2×2 equalizer and CPR are used for real-time hardware processing, and the proposed method are only utilized for imbalance calibration and monitoring, which could be realized by software at microprocessor in practical application. Based on the estimated imbalance factors, gain imbalance, phase imbalance and skew for each polarization could be compensated by simple few-taps real-valued FIR filters, respectively.

III. SIMULATION AND RESULTS

In this section, the proposed scheme is numerically investigated in a 42 GBaud PDM 16-QAM transmission system by using VPItransmissionMaker simulation software, as shown in Fig. 1 (a). The signal processing in the transmitter consists of 2^{20} PRBS data generation, 16-QAM symbol mapping, two times up-sampling, Nyquist pulse shaping with roll-off factor of 0.15. Skew is added after DAC and driving amplifier. $EDFA_1$ without noise after dual-polarization IQ modulator is used to adjust the launch power. The signal is transmitted over a recirculating loop, which consists of a 100-km SSMF with attenuation, CD, PMD and nonlinear coefficient of 0.2 dB/km, 16 ps/nm/km, 0.5 ps/$\sqrt{km}$ and 1.3 $W^{-1}km^{-1}$, an $EDFA_2$ with gain and noise figure of 20 dB and 4 dB, and a BPF with bandwidth of 0.5 nm. After 1500-km transmission, $EDFA_3$ without noise is used to adjust the received power to −10 dBm. Receiver skew module after coherent receiver are used to set time delay. Two samples per symbol after

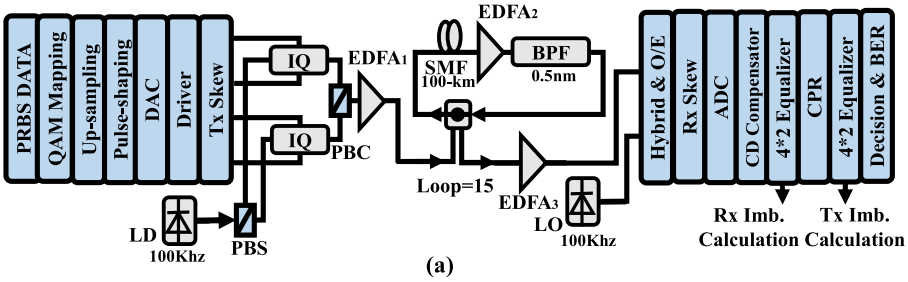

	$\alpha_{TX/TY}$ or $\alpha_{RX/RY}$	$\delta_{TX/TY}$ or $\delta_{RX/RY}$	$\tau_{TX/TY}$ or $\tau_{RX/RY}$
TX1	0 dB	0 deg.	0 ps
TX2	0.25 dB	-2.5 deg.	-2.5 ps
TX3	0.50 dB	-5.0 deg.	-5.0 ps
RX1	0 dB	0 deg.	0 ps
RX2	0.25 dB	-2.5 deg.	2.5 ps
RX3	0.50 dB	-5.0 deg.	5.0 ps

(b)

FIGURE 1. (a) Simulation setup. (PRBS: pseudo-random binary sequence, DAC: digital-to-analog converter, LD: laser, PBS: polarization beam splitter, PBC: polarization beam coupler, EDFA: erbium-doped fiber amplifier, BPF: band-pass filter, LO: local oscillator, ADC: analog-to-digital converter.) (b) The imbalance parameter setups of three TXs and three RXs.

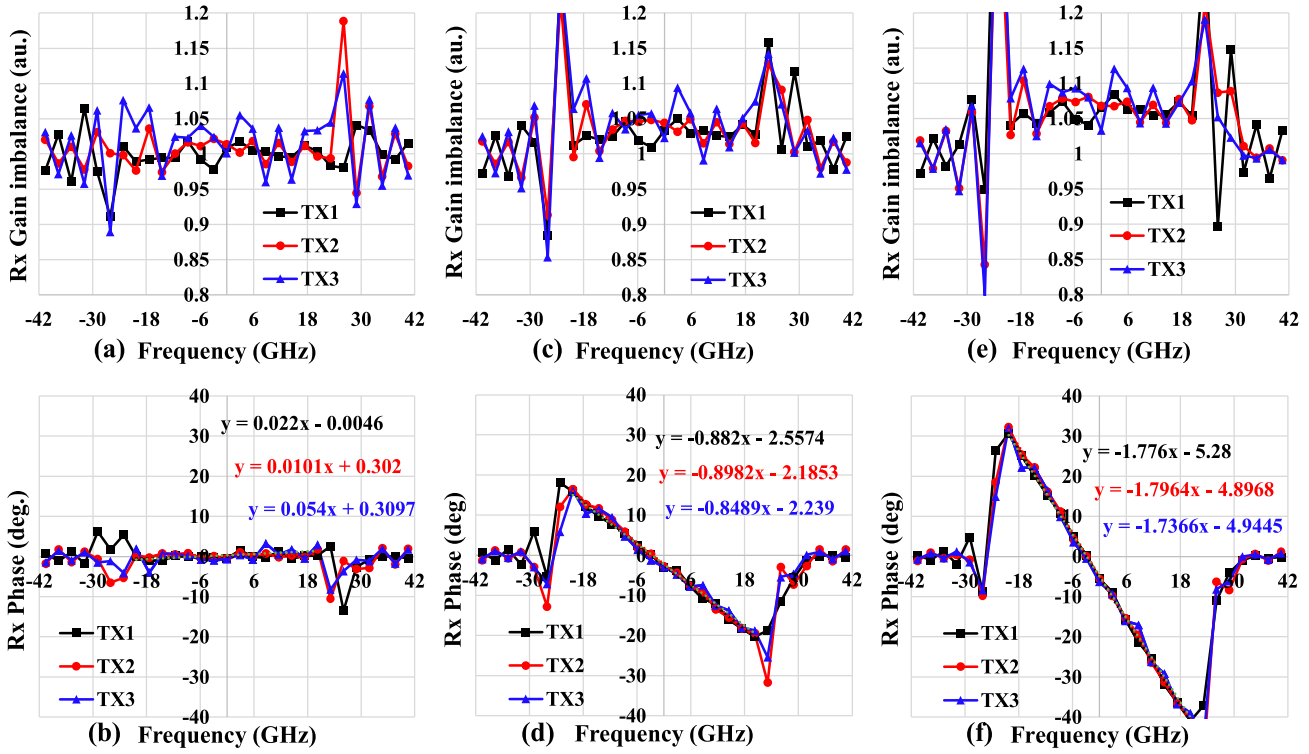

FIGURE 2. Estimated gain imbalance of (a) RX1, (c) RX2, and (e) RX3 with TX1, TX2 and TX3. Estimated phase of (b) RX1, (d) RX2 and (f) RX3 with TX1, TX2 and TX3.

ADC are employed for the following DSP processing, which composes of four CD compensators, RDE-based 4×2 equalizer with 29 taps, pre-decision angle differential estimation (PADS) [17] and Viterbi-Viterbi based CPR, DD-LMS-based 4×2 equalizer with 29 taps, two times down-sampling, symbol decision, bit error rate (BER) and Q factor calculation. Residual CD of 16 ps/nm after four CD compensators is processed by the first 4×2 equalizer. Frequency offset and laser linewidth of transceiver are 200 MHz and 100 KHz, respectively.

In the subsequent evaluation, three different transmitters and three different receivers are used. The detailed imbalance parameter settings are shown in Fig. 1 (b). The impact of transmitter imbalance on the estimation of receiver imbalance is evaluated at launch power of −1 dBm. The estimated gain imbalance and phase of frequency response difference of RX1 for X Pol. with three different transmitters are shown in Fig. 2 (a) and (b). Fig. 2 (c) and (d), (e) and (f) re for the cases of RX2 and RX3. The estimated receiver gain imbalance, phase imbalance, and skew are shown in Table 1. In the presence of transmitter imbalance, receiver imbalance can still be estimated from the converged tap coefficients and the estimation error is less than 0.17 dB, 0.3 deg., 0.2 ps for one measurement. Then, the impact of receiver imbalance on the estimation of transmitter imbalance is evaluated, as shown in Fig. 3 (a–f). The estimated transmitter gain imbalance, phase imbalance, and skew are shown in Table 2. In the presence of receiver imbalance, transmitter imbalance can still be estimated from converged tap coefficients and the estimation error is less than 0.21 dB, 1 deg., 0.23 ps for one measurement.

TABLE 1. The estimated gain imbalance, phase imbalance and skew of rx for one measurement.

		$\alpha_{RX/RY}$	$\delta_{RX/RY}$	$\tau_{RX/RY}$
TX1	RX1	0.01 dB	0.00 deg.	-0.06 ps
TX2		0.04 dB	0.00 deg.	-0.03 ps
TX3		0.17 dB	0.3 deg.	-0.15 ps
TX1	RX2	0.24 dB	-2.55 deg.	-2.45 ps
TX2		0.28 dB	-2.18 deg.	-2.49 ps
TX3		0.41 dB	-2.24 deg.	-2.36 ps
TX1	RX3	0.49 dB	-5.28 deg.	-4.93 ps
TX2		0.53 dB	-4.89 deg.	-4.99 ps
TX3		0.66 dB	-4.94 deg.	-4.82 ps

TABLE 2. The estimated gain imbalance, phase imbalance and skew of tx for one measurement.

		$\alpha_{TX/TY}$	$\delta_{TX/TY}$	$\tau_{TX/TY}$
TX1	RX1	-0.01 dB	0.22 deg.	0.08 ps
	RX2	0.00 dB	-0.24 deg.	0.00 ps
	RX3	0.00 dB	0.04 deg.	0.06 ps
TX2	RX1	0.16 dB	-2.24 deg.	-2.41 ps
	RX2	0.23 dB	-2.11 deg.	-2.45 ps
	RX3	0.17 dB	-2.83 deg.	-2.38 ps
TX3	RX1	0.29 dB	-5.31 deg.	-4.78 ps
	RX2	0.31 dB	-6.07 deg.	-4.77 ps
	RX3	0.40 dB	-5.83 deg.	-4.81 ps

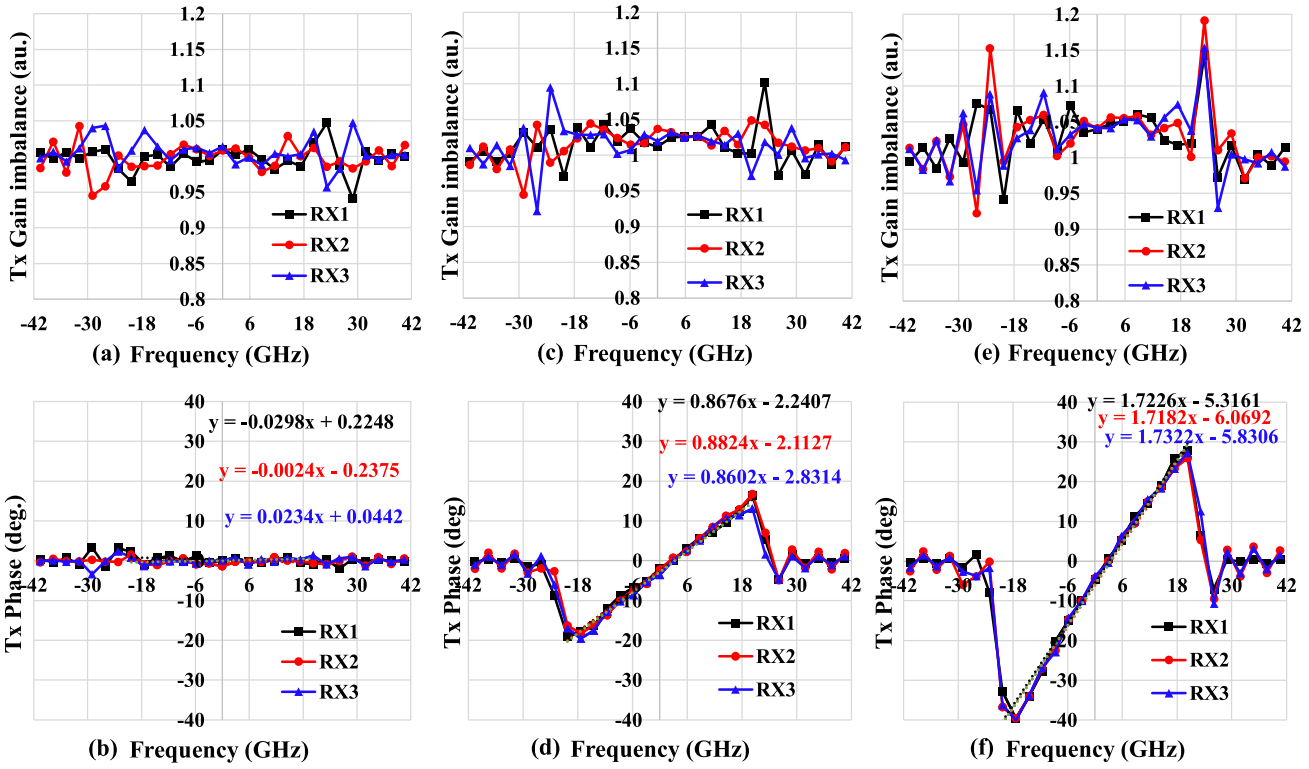

FIGURE 3. Estimated gain imbalance of (a) TX1, (c) TX2, and (e) TX3 with RX1, RX2 and RX3. Estimated phase of (b) TX1, (d) TX2 and (f) TX3 with RX1, RX2 and RX3.

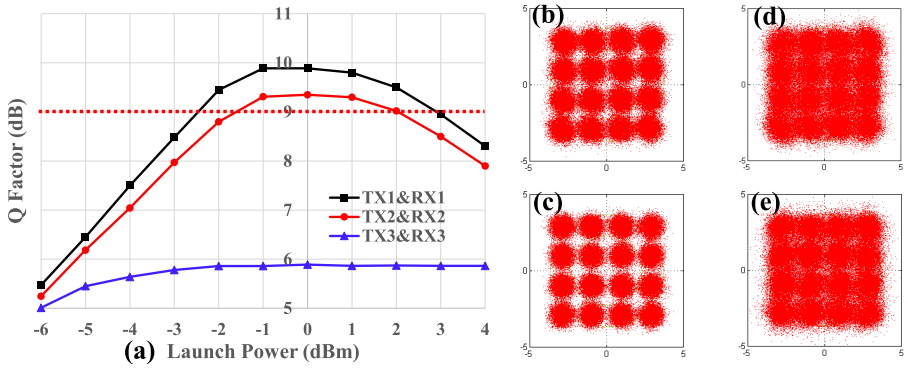

FIGURE 4. (a) Q factor verus launch power after 1500-km SSMF transmission with different transceiver setup: TX1&RX1, TX2&RX2 and TX3&RX3. Constellation (b) before and (c) after DD-LMS based 4×2 equalizer for the case of TX2&RX2 at launch power of −1 dBm. Constellation (d) before and (e) after DD-LMS based 4×2 equalizer for the case of TX3&RX3 at launch power of −1 dBm.

Fig. 4. (a) shows the measured Q factor versus the launch power after 1500-km SSMF transmission with three different transceivers. The case of TX1&RX1 has no transceiver imbalance, which is used as a reference. The optimal launch power for the cases of TX1&RX1 and TX2&RX2 is −1 dBm. Constellations before and after DD-LMS based 4×2 equalizer are shown in Fig. 4 (b) and (c), (d) and (e) for the cases of TX2&RX2 and TX3&RX3, respectively. The signal quality for TX2&RX2 shown in (c) is significantly improved. However, almost no improvement is observed for TX3&RX3 shown in (e). The reason is that the error signal for updating the tap coefficients using RDE algorithm is calculated as $e = \left|\hat{d}\right|^2 - |\text{out}|^2$, where $\hat{d}$ is the symbol decided from equalizer output, *out*. Transmitter imbalance reduces the accuracy of symbol decision, and further impacts the estimation accuracy of equalizer taps. The residual Rx imbalance and channel linear interference further affects the performance of the DD-LMS based 4×2 equalizer. Q penalty of 0.6 and 4 dB is reduced at launch power of −1 dBm for the case of TX2&RX2 and TX3&RX3, respectively.

The theory modeling does not consider fiber nonlinearity. Nevertheless, nonlinearity is a major bottleneck for long-haul transmission. The detrimental effect of nonlinearity on the estimation of transceiver imbalance is evaluated. It can

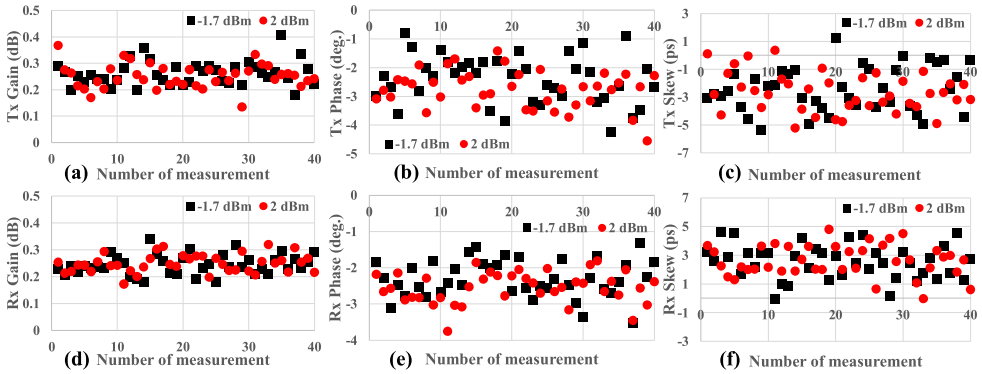

FIGURE 5. Transmitter (a) gain, (b) phase, (c) skew estimation and receiver (d) gain, (e) phase, (f) skew estimation after 1500-km SSMF transmission at launch power of −1.7 dBm and 2 dBm with 40 measurements.

be found from Fig. 4 (a) that the same Q values (Q=9 dB, corresponding to the FEC limit) are observed at launch power of −1.7 dBm and 2 dBm for the case of TX2&RX2, respectively. The main system bottleneck at launch power of 2 dBm is fiber nonlinearity. Transceiver imbalance estimation with 40 measurements are shown in Fig. 5. The mean value and variance of transmitter gain imbalance, phase imbalance and skew are 0.24 dB and 0.03, −2.31 deg. and 0.5, −2.54ps and 1.19, for the case with launch power of −1.7 dBm, 0.25 dB and 0.03, −2.54 deg. and 0.43, −2.6 ps and 1.1, for the case with launch power of 2 dBm. The mean value and variance of receiver gain imbalance, phase imbalance and skew are 0.25 dB and 0.04, −2.75 deg. and 0.65, 2.67 ps and 1.4, for the case with launch power of −1.7 dBm, 0.26 dB and 0.05, −2.4 deg. and 0.85, 2.44 ps and 1.6, for the case with launch power of 2 dBm. Therefore, from the above results, accuracy of measurement for the case at weak nonlinearity (launch power of −1.7 dBm) and strong nonlinearity (launch power of 2 dBm) with the same Q value are almost the same.

IV. CONCLUSION

In this work, channel modeling is given to analyze the interaction of transceiver imbalance and fiber link for long-haul fiber transmission. RDE- and DD-LMS-based 4×2 equalizers operating at twice symbol rates before and after CPR are designed to mitigate the channel linear interference including receiver imbalance, and the transmitter imbalance, respectively. Transceiver imbalance can be derived from the converged two equalizers taps, which can be utilized to calibrate and monitor the transceiver status. The measurement accuracy caused by the transceiver imbalance and fiber nonlinearity are analyzed in a 42 GBaud 16-QAM system through 1500-km SSMF transmission.

REFERENCES

[1] W. Shieh, H. Bao, and Y. Tang, "Coherent optical OFDM: Theory and design," *Opt. Express*, vol. 16, no. 2, pp. 841–859, 2008.

[2] I. Fatadin, S. J. Savory, and D. Ives, "Compensation of quadrature imbalance in an optical QPSK coherent receiver," *IEEE Photon. Technol. Lett.*, vol. 20, no. 20, pp. 1733–1735, Oct. 15, 2008.

[3] R. Rios-Müller, J. Renaudier, and G. Charlet, "Blind receiver skew compensation and estimation for long-haul non-dispersion managed systems using adaptive equalizer," *J. Lightw. Technol.*, vol. 33, no. 7, pp. 1315–1318, Apr. 2015.

[4] E. Porto da Silva and D. Zibar, "Widely linear equalization for IQ imbalance and skew compensation in optical coherent receivers," *J. Lightw. Technol.*, vol. 34, no. 15, pp. 3577–3586, Aug. 1, 2016.

[5] M. S. Faruk and K. Kikuchi, "Compensation for in-phase/quadratureimbalance in coherent-receiver front end for optical quadrature amplitude modulation," *IEEE Photon. J.*, vol. 5, no. 2, Apr. 2013, Art. no. 7800110.

[6] M. Paskov, D. Lavery, and S. J. Savory, "Blind equalization of receiver in-phase/quadrature skew in the presence of Nyquist filtering," *IEEE Photon. Technol. Lett.*, vol. 25, no. 24, pp. 2446–2449, Dec. 15, 2013.

[7] N. Stojanovic and X. Changsong, "An efficient method for skew estimation and compensation in coherent receivers," *IEEE Photon. Technol. Lett.*, vol. 28, no. 4, pp. 489–492, Feb. 2016.

[8] *Optical Internetworking Forum (OIF)*, document OIF-CFP2-ACO-01.0, 2016.

[9] C. Ju, Z. Tao, Y. Y. Fan, Y. Zhao, H. Chen, X. F. Su, and T. Hoshida, "Calibration of in-phase/quadrature amplitude and phase response imbalance for coherent receiver," in *Proc. Opt. Fiber Commun. Conf. (OFC)*, Mar. 2017, pp. 1–3, Paper W2A.55.

[10] G. Khanna, S. Calabro, B. Spinnler, E. de Man, and N. Hanik, "Joint adaptive pre-compensation of transmitter I/Q skew and frequency response for high order modulation formats and high baud rates," in *Proc. Opt. Fiber Commun. Conf. (OFC)*, Mar. 2015, pp. 1–3, Paper M2G.4.

[11] C. R. S. Fludger and T. Kupfer, "Transmitter impairment mitigation and monitoring for high baud-rate, high order modulation systems," in *Proc. Eur. Conf. Exhib. Opt. Commun. (ECOC)*, Sep. 2016, pp. 256–258.

[12] T. H. Nguyen, P. Scalart, M. Gay, L. Bramerie, C. Peucheret, T. Nguyen-Ti, M. Gautier, O. Sentieys, J. C. Simon, and M. Joindot, "Blind adaptive transmitter IQ imbalance compensation in M-QAM optical coherent systems," in *Proc. IEEE Int. Conf. Commun. (ICC)*, May 2016, pp. 1–6.

[13] C. R. S. Fludger, T. Duthel, P. Hermann, and T. Kupfer, "Low cost transmitter self-calibration of time delay and frequency response for high baud-rate QAM transceivers," in *Proc. Opt. Fiber Commun. Conf. Exhib. (OFC)*, Mar. 2017, pp. 1–3, Paper Th1D.3.

[14] Y. Yue, B. Zhang, Q. Wang, R. Lofland, and J. O'Neil, and J. Anderson, "Detection and alignment of dual-polarization optical quadrature amplitude transmitter IQ and XY skews using reconfigurable interference," *Opt. Express*, vol. 24, no. 6, pp. 6719–6734, 2016.

[15] J. C. M. Diniz, F. D. Ros, R. T. Jones, and D. Zibar, "Time skew estimator for dual-polarization QAM transmitters," in *Proc. Eur. Conf. Exhib. Opt. Commun. (ECOC)*, Sep. 2017, pp. 1–3.

[16] Q. Zhang, Y. Yang, C. Guo, X. Zhou, Y. Yao, A. P. T. Lau, and C. Lu, "Algorithms for blind separation and estimation of transmitter and receiver IQ imbalances," *J. Lightw. Technol.*, vol. 37, no. 10, pp. 2201–2208, May 15, 2019.

[17] L. Li, Z. Tao, S. Oda, T. Hoshida, and J. C. Rasmussen, "Wide-range, accurate and simple digital frequency offset compensator for optical coherent receivers," in *Proc. Conf. Opt. Fiber Commun./Nat. Fiber Optic Eng. Conf.*, Feb. 2008, pp. 1–3.

CHENG JU received the Ph.D. degree in communication and information system from the Beijing University of Posts and Telecommunications (BUPT), Beijing, China, in 2015. In 2015, he joined the Fujitsu Research and Development Center, Beijing, where he has been engaged in the research and development for next generation Tb/s coherent communication. In 2018, he joined the College of Electronic Information, Qingdao University. His research interests include transceiver imbalance monitoring, low-complexity DSP algorithm, and real-time coherent optical transmission systems. He was awarded the Excellent Doctoral Thesis Award of BUPT.

NA LIU received the Ph.D. degree from the Beijing University of Posts and Telecommunications, Beijing, China, in 2015. She then joined the College of Electronic Information, Qingdao University. Her research interests include passive optical networks, optical orthogonal frequency-division multiplexing transmission systems, and long-reach optical interconnects.

CHANGHONG LI received the Ph.D. degree from the Beijing University of Posts and Telecommunications, Beijing, China, in 2008. In 2008, she joined the College of Electronic Information, Qingdao University. Her current research interests include impairment compensation in intensity modulation and direction detection systems, and channel equalization in underwater optical transmission systems.